Pyk2 Overexpression in Postsynaptic Neurons Blocks $A\beta_{1-42}$-induced Synaptotoxicity in a Microfluidic Co-Culture Model

Devrim Kilinc[a]*, Anaïs-Camille Vreulx[a], Tiago Mendes[a], Amandine Flaig[a], Maxime Verschoore[a], Florie Demiautte[a], Philippe Amouyel[a], Fanny Eysert[a], Pierre Dourlen[a], Julien Chapuis[a], Nicolas Malmanche[a], Frederic Checler[b] and Jean-Charles Lambert[a]*

[a] INSERM U1167 Laboratory of Excellence: "Distalz", Institut Pasteur de Lille, Université de Lille. 1 rue du Prof Calmette, BP245, Lille 59019 France
[b] CNRS UMR727 Laboratory of Excellence "Distalz", IPMC, Université Côte d'Azur, Inserm. 660 Route des Lucioles, Sophia-Antipolis, Valbonne 06560 France
* Corresponding authors: devrim.kilinc@pasteur-lille.fr; jean-charles.lambert@pasteur-lille.fr

Recent meta-analyses identified a number of genetic risk factors of Alzheimer's disease (AD); however, little is known about the mechanisms by which they contribute to the pathological process. As synapse loss is observed at the earliest stage of AD, deciphering the impact of AD risk genes on synapse formation and maintenance is of great interest. In this paper, we report a microfluidic co-culture device that physically isolates synapses from pre- and postsynaptic neurons and chronically exposes them to toxic amyloid-beta (Aβ) peptides secreted by model cell lines overexpressing wild-type or mutated (V717I) amyloid precursor protein (APP). Co-culture with cells overexpressing mutated APP exposed the synapses of primary hippocampal neurons to $A\beta_{1-42}$ molecules at physiologically-relevant concentrations and induced a significant decrease in synaptic connectivity, as evidenced by distance-based assignment of postsynaptic puncta to presynaptic puncta. Treating the cells with antibodies that target different forms of Aβ suggested that low molecular weight oligomers are the likely culprit. As proof of concept, we demonstrate that overexpression of Pyk2 –an AD risk gene involved in synaptic plasticity– selectively in postsynaptic neurons is protective against $A\beta_{1-42}$-induced synaptotoxicity. In summary, our lab-on-a-chip device provides a physiologically-relevant model of AD-related synaptotoxicity, optimal for assessing the impact of risk genes in pre- and postsynaptic compartments.

Introduction

Alzheimer's disease (AD), the most common neurodegenerative disorder worldwide, is characterized by two types of brain lesions: (i) neurofibrillary degeneration due to the intracellular aggregation of abnormally hyperphosphorylated tau protein and (ii) amyloid plaques resulting from the extracellular accumulation of amyloid beta (Aβ) peptides.[1] Aβ peptides are generated by the cleavage of the transmembrane amyloid precursor protein (APP) and can have different residue lengths.[2] The discovery of mutations in the APP, PS1 and PS2 genes (coding for APP and presenilins 1 and 2) causing early-onset, autosomal-dominant forms of AD has profoundly influenced our understanding of the disease, and has placed Aβ peptides at the center of the pathophysiological process. According to the "amyloid cascade hypothesis", the accumulation of Aβ peptides is the triggering toxic condition that induces the development of neurofibrillary degeneration and thus neuronal death.[3]

$A\beta_{1-42}$ species have been the principal focus of research [4] since $A\beta_{1-42}$ is more prone to oligomerize [5, 6] and oligomers of $A\beta_{1-42}$ are more toxic than its monomeric or fibrillary forms, and other Aβ species.[7-9] Oligomeric $A\beta_{1-42}$ is in a dynamic equilibrium with the monomeric forms and fibrils, and has been proposed to be the main promoter of amyloid plaques.[10] Even if the central role of the Aβ peptide burden as initially enunciated in this hypothesis is strongly debated, several lines of evidence indicate that Aβ peptides are still a key actor

of the disease at least via their oligomeric forms. In particular, the Aβ oligomer toxicity has been linked with synapse dysregulation and loss.[11]

Synapse loss is a major pathological correlate of cognitive deficits in AD [12] and is observed at the earliest stage of the disease.[13] Several mechanisms have been proposed to explain Aβ-induced synaptotoxicity: (i) membrane-disrupting activity at high concentrations;[14] (ii) deleterious pruning of synapses by microglia activation;[15] (iii) direct interaction of oligomeric forms with postsynaptic receptors, such as ionotrophic or metabotropic glutamate receptors.[16, 17] In addition, the new genetic landscape of AD, resulting from the advent of the genome wide association studies (GWAS),[18, 19] highlights synaptic (dys)regulation: several among the dozens of genes/loci identified to be associated with AD risk, *e.g.*, *BIN1*, *CD2AP*, *FERMT2* and *PTK2B*, have been shown to modulate synaptic functions in the physio- and/or pathophysiological contexts.[20-24] As a result, we recently proposed a genetically-driven synaptic failure hypothesis, based on the genetic and post-GWAS data.[25] In this context, Aβ toxicity is one of the elements involved in synapse failure and it may be driven by specific AD genetic risk factors.

However, assessing such an hypothesis requires a number of considerations to be taken into account: (i) most *in vitro* models of Aβ toxicity use synthetic Aβ oligomers at non-physiological concentrations, even though synthetic fibrils are structurally different from Aβ fibrils obtained from AD brains;[26] (ii) only a few of the GWAS-defined genes have been analyzed in a (physiological and/or pathophysiological) synaptic context; (iii) GWAS-defined genes may have different effects when expressed in the pre- or postsynaptic neurons. For example, proline-rich tyrosine kinase 2 (Pyk2), product of AD risk gene *PTK2B*, directly interacts with postsynaptic scaffold proteins,[27] regulates dendritic spine morphology,[20] and is involved in synaptic plasticity through regulating postsynaptic NMDA receptors via activation of Src.[28] Recent studies based on AD mouse models linked Pyk2's effects to amyloid pathology, but reported contradictory data on whether lack of Pyk2 was detrimental or protective.[23, 29]

With this background, we have developed a microfluidic co-culture device, based on existing tricompartment designs that physically isolate synapses and provide exclusive access to pre- and postsynaptic neurons.[30, 31] This device permits not only the induction of synaptotoxicity via physiologically-relevant concentrations of Aβ molecules secreted by cells stably overexpressing human APP, but also the analysis of synaptic density as a function of over- or underexpression of genetic risk factors in pre- and/or postsynaptic neurons. In this paper, we characterize synaptotoxicity in primary neurons upon co-culture with cells overexpressing mutated APP and assess the impact of Pky2 overexpression in postsynaptic neurons, as a proof of concept.

Results and Discussion

Microfluidic co-culture device to expose hippocampal synapses to synthetic or cell secreted Aβ oligomers

With the goal to better mimic AD *in vitro*, we developed a microfluidic device that permits synapse formation between two sets of neurons cultured in distinct chambers. Based on a previous design, our device consists of three distinct chambers, interconnected *via* parallel microchannels that constrain neuronal cell bodies but permit axons and dendrites to cross through (Fig. 1).[32] Adjusting the lengths of microchannels made it possible to allow axons and dendrites from the right (or "postsynaptic") chamber, but only axons from the left (or "presynaptic") chamber to reach the central (or "synaptic") chamber (Fig. 1C).[30] As a novel design feature, one end of the synaptic chamber bifurcates, where one branch terminates with an access well and the other one connects to a fourth (co-culture) chamber via a dense series of short microchannels. In addition, we employed narrowing microchannels that promote unidirectional neurite crossing.[33] When rat postnatal hippocampal neurons were cultured in one chamber only (Fig. S1), 2.9× more axons crossed the long

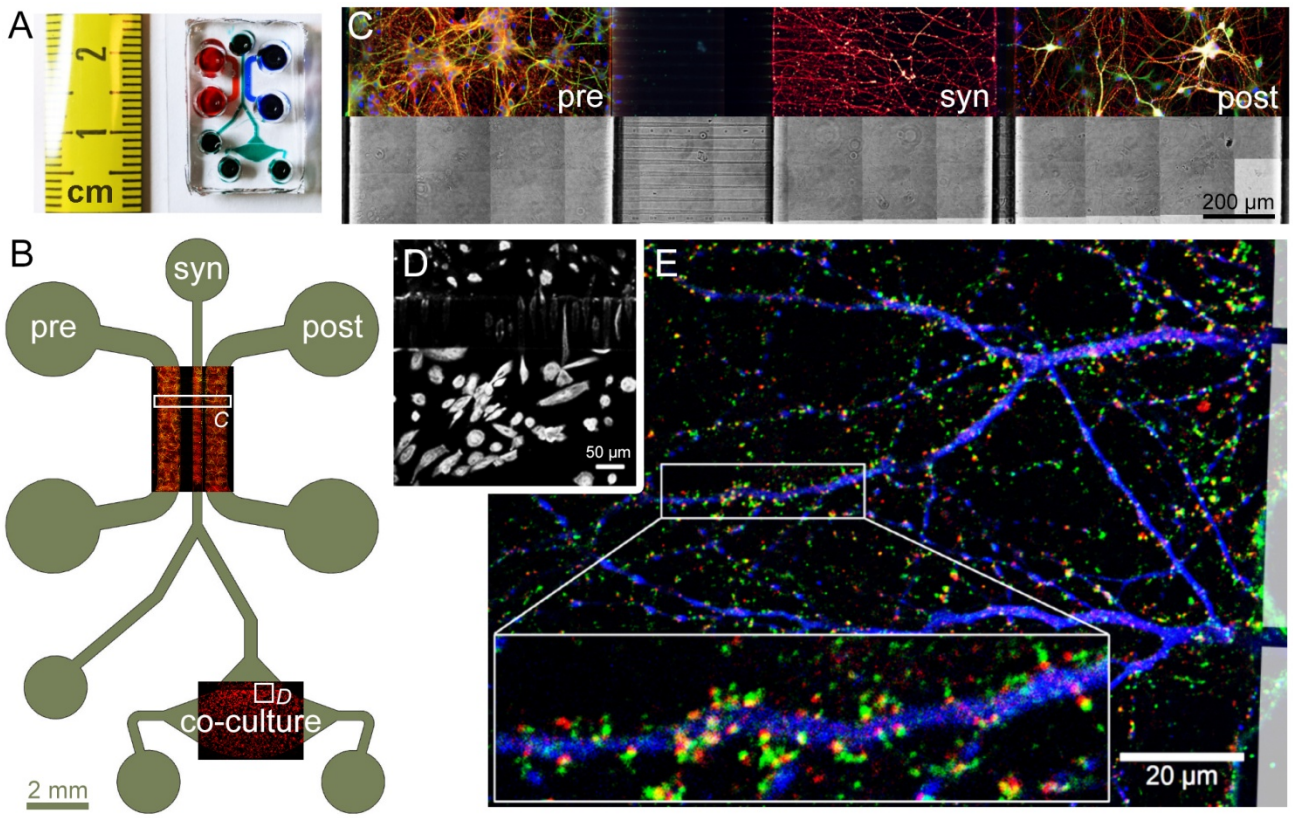

Figure 1. Design and operating principle of the microfluidic co-culture device. **A.** Photograph of the microfluidic device bonded to a coverslip. **B**. The layout of the device showing the presynaptic (pre), synaptic (syn), and postsynaptic (post) chambers, as well as the co-culture chamber housing the CHO cells. Overlays show immunofluorescence images of primary neurons and CHO cells in their respective chambers, stained for α-tubulin (red) and MAP2 (green). **C.** Subcellular compartmentalization of neurons was shown by immunostaining against β3-tubulin (red) and MAP2 (green), axonal and somatodendritic markers, respectively. Cell bodies were stained with Hoechst (blue). Microchannel structure is evident in the brightfield image of the same area. **D.** 15× magnification of the square marked in (B), showing CHO cells cultured in the co-culture chamber. CHO cells pass through the microchannels, but do not migrate up the synaptic channel. **E.** Synapse formation in the synaptic chamber was evidenced by the localization of Synaptopysin 1 (green) and Homer 1 (red) puncta, pre- and postsynaptic markers, respectively, around MAP2-positive dendrites (blue). Boxed area is 3× magnified.

microchannels in the forward direction (from the wide end towards the narrow end) than the reverse direction. This figure decreased to 1.9× in the case of short microchannels. These ratios are indicative of a limited effect of the narrowing channel design on hippocampal neurons and are consistent with earlier reports.[33]

At 14 days *in vitro* (DIV14), no dendrites emanating from neurons cultured in the presynaptic chamber were observed in the synaptic chamber. Axons from these neurons, however, invaded the entire synaptic chamber. 11.0%±4.0% of these axons crossed the short microchannels in the reverse direction and reached the postsynaptic chamber, as measured by the ratio of the β3-tubulin fluorescence between the emitting and receiving chambers. On the other hand, axons and dendrites from neurons cultured in the postsynaptic chamber fully invaded the synaptic chamber by DIV14. None of these dendrites and only 5.9%±1.6% of these axons crossed the long microchannels in the reverse direction and reached the presynaptic chamber. Synapse formation in the synapse chamber was confirmed by immunostaining against Synaptophysin (Syp) 1 and Homer 1, pre- and postsynaptic markers, respectively (Fig. 1E). In summary, the synaptic chamber receives axons from both pre- and postsynaptic chambers, receives dendrites only from the postsynaptic chamber, and contains 83.2%±6.1% of all synaptic connections formed between pre- and postsynaptic chambers.

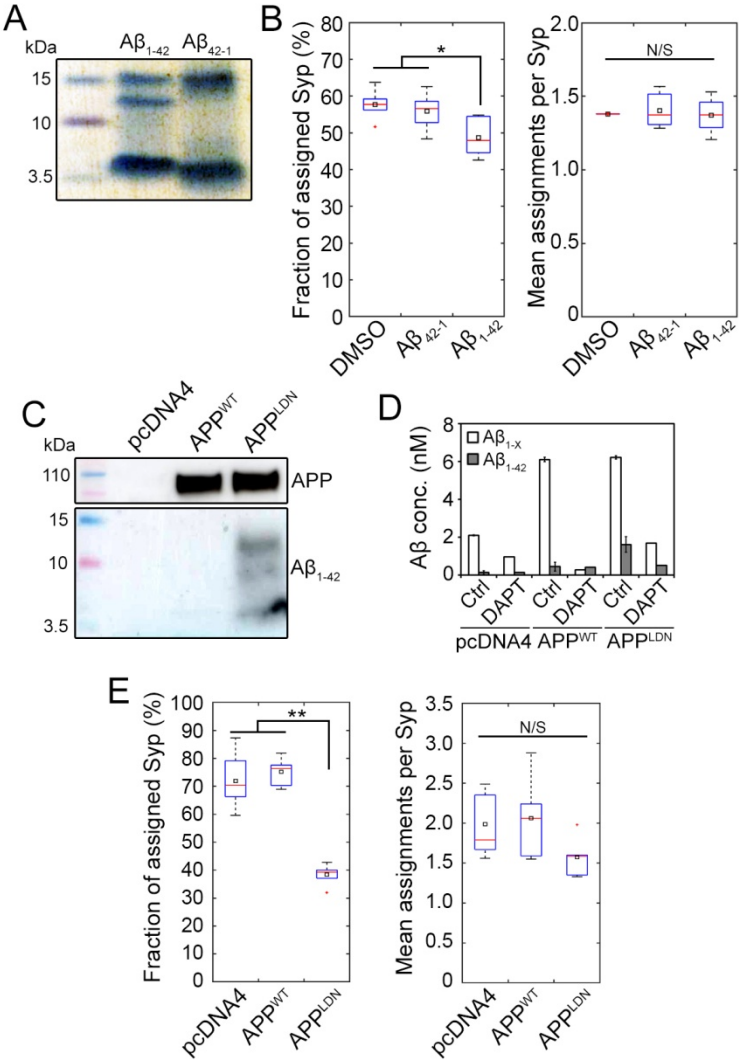

Figure 2. Synthetic and cell-secreted $A\beta_{1-42}$ induce different levels of synaptic toxicity. **A.** Coomassie blue stain of in-house oligomerized synthetic $A\beta_{1-42}$ and $A\beta_{42-1}$ (inverted control) peptides show the presence of low molecular weight oligomers. **B.** Synaptic read-outs 16 h after the introduction of synthetic oligomer solution into the synaptic chamber at DIV14 (final concentration = 100 nM). Fraction of Syp puncta assigned by Homer puncta and the mean number of Homer puncta assigned per Syp, according to distance-based analysis workflow (see Fig. S1 for details). **C.** Immunoblots of CHO cell media two days after stimulation. **D.** Alpha-LISA measurement of $A\beta_{1-X}$ and $A\beta_{1-42}$ in media collected from the top well of the synaptic chamber at DIV14. γ-secretase inhibitor DAPT was applied at 18 µg/mL for 5 d. **E.** Synaptic read-outs following co-culture with CHO cells (at DIV 14). In box plots, red bars, black squares, and red plus signs indicate sample median and mean, and outliers, respectively. In panel *B*, N = 5-6 devices from at least 3 independent cultures. In panel *E*, N = 6-7 microfluidic devices from 3 independent cultures. Kruskal-Wallis ANOVA, followed by Wilcoxon rank-sum test. * $p < 0.05$; ** $p < 0.005$; N/S: not significant.

Effect of synthetic $A\beta_{42}$ oligomers on synapse connectivity

We oligomerized synthetic $A\beta_{1-42}$ and $A\beta_{42-1}$ (inverted control peptide) and assessed the presence of oligomeric species *via* Coomassie blue staining. We confirmed the presence of low-MW oligomers in the $A\beta_{1-42}$ sample (Fig. 2A). We exposed mature synapses (DIV14) to synthetic Aβ peptides by adding the oligomer solution to the synapse chamber to reach an initial concentration of 100 nM. We kept the media levels in the synaptic reservoirs lower than those in the pre- and postsynaptic reservoirs. The hydrostatic pressure difference induced a flow through the microchannels countering the molecular diffusion, which localized the

treatment initially to the synaptic chamber. However, as the pressure-driven flow ceased, the media levels equilibrated and Aβ peptides diffused throughout the device. Since the short microchannels offer little fluidic resistance compared to the long microchannels, it would be safe to assume that the media levels equilibrated first between the synaptic and postsynaptic chambers and then between the synaptic and presynaptic chambers.

At the end of the 16 h treatment period, the neurons were fixed and immunostained against pre- and postsynaptic markers. To quantitatively analyze synaptic connectivity, we developed an image analysis workflow based on scanning confocal microscopy, software-assisted identification of pre- and postsynaptic puncta, and proximity-based assignment of postsynaptic puncta to presynaptic puncta (Fig. S2). Briefly, each Homer spot was assigned to the nearest Syp spot within a cut-off distance, which was pre-determined using a training set (Fig. S2G). The fraction of Syp puncta with at least one Homer assignments and the average number of Homer assignments per Syp were determined to be the most robust read-outs of synapse connectivity. Exposing synapses to synthetic $A\beta_{1-42}$ oligomers decreased the fraction of assigned Syp without affecting the average number of assignments (Fig. 2B). However, the effect size was small (15.6%) and the variation within and among experiments was high.

Co-culture with CHO cells expressing human APP with London mutation (V717I) induces synaptotoxicity

We cultured Chinese hamster ovary (CHO) cell lines stably overexpressing human APP, either wild-type ($CHO\text{-}APP^{WT}$) or with V717I (London) mutation ($CHO\text{-}APP^{LDN}$). It has been shown that $CHO\text{-}APP^{WT}$ and $CHO\text{-}APP^{LDN}$ continuously secrete physiologically-relevant forms of Aβ molecules and $CHO\text{-}APP^{LDN}$ provides toxic Aβ species.[34] Immunoblot analysis of media collected from CHO cell cultures confirmed that only the peptides secreted by $CHO\text{-}APP^{LDN}$ formed low-MW oligomers (Fig. 2C). In contrast, CHO-pcDNA4 cells, which do not overexpress APP, did not produce any Aβ. We conducted off-chip ELISA measurements to determine the relative levels of Aβ species in CHO cell media (Fig. S3). As expected, treatment with the γ-secretase inhibitor DAPT completely blocked the secretion of Aβ peptides by both $CHO\text{-}APP^{WT}$ and $CHO\text{-}APP^{LDN}$ cells. Moreover, $A\beta_{1-42}$ (but not $A\beta_{1-40}$) levels in $CHO\text{-}APP^{LDN}$ media was higher than in $CHO\text{-}APP^{WT}$ media, further supporting the immunoblot results.

To determine the effect of CHO cell-secreted Aβ forms on synapses, we plated *ca.* 10,000 CHO cells in the co-culture chamber 4-6 days prior to the primary neuron culture. This timing was necessary to overcome the problems invoked by the differences of growth media composition between CHO cells and primary neurons. CHO cells proliferated in their growth medium and fully occupied the co-culture chamber. CHO cells were able to cross the short microchannels separating the co-culture chamber from the synaptic chamber (Fig. 1D), but they did not migrate up the synaptic chamber. When the growth medium was replaced with the stimulation medium, the cells stopped proliferating, but continued to secrete Aβ peptides. To confirm that CHO cell-secreted Aβ forms diffused into the synaptic chamber, we collected media from different media reservoirs and quantified their $A\beta_{1-X}$ and $A\beta_{1-42}$ peptide content using corresponding Alpha-LISA kits. Note that media collected from the wells of the microfluidic device did not contain sufficient material for immunoblotting. Measurements taken at DIV14 revealed that the ratio of $A\beta_{1-42}$ to other Aβ forms in the synaptic chamber was 4.4-fold higher in $CHO\text{-}APP^{LDN}$ co-cultures than in CHO- APP^{WT} co-cultures (Fig. 2D), as expected for the overexpression of mutated APP.[34] Aβ forms in the media decreased to undetectable levels when CHO cells were treated with γ-secretase inhibitor DAPT for 5 d prior to media collection, further confirming that the majority of the measured Aβ in the synaptic chamber was secreted by the CHO cells. Presence of $A\beta_{1-X}$ in media collected from the synaptic chamber, but not in the co-culture chamber of the CHO-pcDNA4 co-cultures is indicative of neuronal APP processing, since these cells do not express APP and do not secrete Aβ peptides (Fig. S4).

We conducted off-chip experiments to assess the availability of cell-secreted Aβ forms following the addition of the conditioned media to primary neuron cultures. Alpha-LISA measurements conducted at different time points (from 6 h to 7 d) suggested that Aβ concentrations in the media decreased logarithmically over time (Fig. S5), suggesting that the peptides degraded or consumed by the cells. In contrast, the concentration of synthetic $A\beta_{1-42}$ peptide did not exhibit such a decrease over time when added to neurons (not shown). These observations further support the idea that cell-secreted Aβ forms need to be periodically resupplied to the neuron culture medium unless a co-culture model is available.

When synapses were exposed to CHO cell-secreted Aβ forms for 14 days in the co-culture device, a strong decrease in synapse connectivity was observed in CHO-APP^{LDN}, but not in CHO-APP^{WT} co-cultures (Fig. 2E). In this case, *i.e.*, following chronic exposure, the effect size was large (45.6%) and the variation within and among experiments was low.

Several parameters can be considered when inducing Aβ-dependent synaptotoxicity: (i) use of synthetic versus organic oligomers; (ii) acute versus chronic treatment. Our microfludic co-culture model combines organic oligomers at physiological concentrations with chronic treatments and consistently induces Aβ-dependent synaptotoxicity. This is in agreement with a recent report that synthetic oligomers do not assume the same molecular structure as organic oligomers,[26] suggesting potential differences in their biological effects. Interestingly, as opposed to synthetic Aβ oligomers, organic Aβ appears to be degraded in our primary neuronal cultures, further highlighting the difference in bioavailability between the two. This observation also indicates that the co-culture model is better adapted for synaptotoxicity studies since it maintains physiological concentrations thanks to the constant release of Aβ peptides from CHO cells. This allows for the analysis of synapse connectivity in response to chronic exposure of synapses to organic Aβ oligomers, as opposed to acute exposure to conditioned media, for instance.

Aβ antibody 3D6 alters the ratio between different Aβ forms and blocks CHO-APP^{LDN}-induced synapse loss

To further characterize the CHO cell-secreted Aβ forms, we tested two monoclonal Aβ antibodies, human SAR228810 (8810; Sanofi; 3 μg/mL) and the mouse version of Bapineuzumab (3D6; Janssen; 3 μg/mL). Both antibodies were developed for passive immunotherapy and tested in clinical trials. 8810 antibody targets soluble protofibrillar and fibrillar species of Aβ and is inactive against Aβ monomers and small oligomeric aggregates.[35] In contrast, the 3D6 antibody targets the N-terminal region of Aβ and expected to capture Aβ molecules in the monomeric conformation.[36, 37]

We first conducted off-chip experiments where CHO cells were treated with these antibodies (or with 18 μg/mL DAPT as a negative control) for 5 d. Western blots of the conditioned media showed that DAPT treatment eliminated all Aβ secretion and induced a slight increase in the levels of APP (Fig. 3A). However, WBs of conditioned media following DAPT treatment exhibited a 15 kDa band that overlapped with oligomers of low MW $A\beta_{1-42}$. Treatment with neither antibody affected the presence of low-MW $A\beta_{1-42}$ forms. Interestingly, the 3D6 antibody induced a strong increase in monomeric $A\beta_{1-42}$ levels in both CHO-APP^{WT} and CHO-APP^{LDN} media, in accordance with the idea that 3D6 arrests the peptide in monomeric form and precludes oligomer formation.

We next performed Alpha-LISA measurements from media collected from the co-culture chamber, following the treatment of CHO cells with the aforementioned antibodies for 5 d. However, the 3D6 antibody interfered with the Alpha-LISA measurements and could not be reported (no effect was observed for 8810 antibody). We therefore conducted off-chip ELISA measurements in the media of antibody-treated CHO cells. Treatment with either antibody increased $A\beta_{1-40}$ in both CHO-APP^{WT} and CHO-APP^{LDN} media. Treatment with 8810 antibody did not affect $A\beta_{1-42}$ in CHO-APP^{LDN} medium, but increased $A\beta_{1-42}$ in CHO-APP^{WT} to the CHO-APP^{LDN} level. In both CHO-APP^{WT} and CHO-APP^{LDN} media, 3D6 antibody treatment caused a decent increase in $A\beta_{1-40}$, but a very large increase in $A\beta_{1-42}$, consistent with the WB data (Fig. 3B). The 3D6

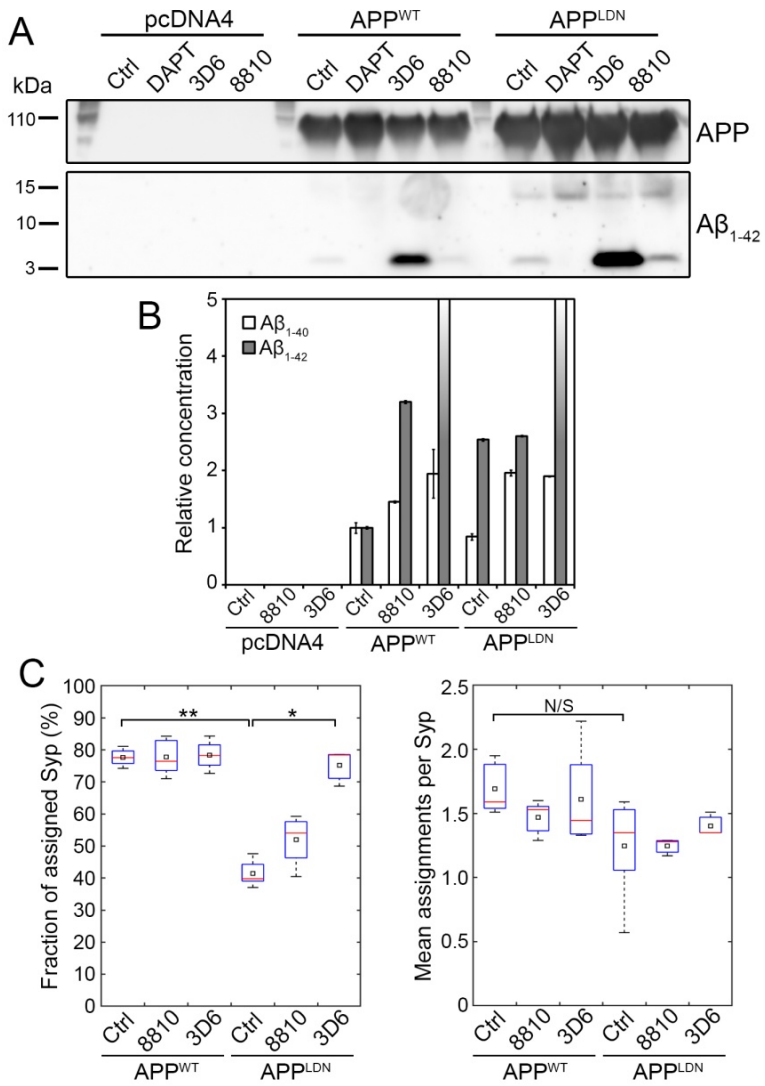

Figure 3. Aβ antibody 3D6 modulates Aβ secretion and blocks the synaptotoxicity due to CHO-APP^{LDN} co-culture. **A.** An exemplary immunoblot of CHO cell media collected after 5 day-long treatment with the indicated compounds (DAPT, 18 µg/mL; antibodies, 3 µg/mL) showing APP cleavage products of different molecular weights. **B.** Off-chip ELISA measurements in CHO cell media following antibody treatment. N = 2 independent experiments. Error bars = SEM. **C.** Synaptic read-outs in antibody-treated co-cultures at DIV 14. In box plots, red bars, black squares, and red plus signs indicate sample median and mean, and outliers, respectively. N = 3-5 microfluidic devices from at least 3 independent cultures. Kruskal-Wallis ANOVA, followed by Wilcoxon rank-sum test. * $p < 0.05$; ** $p < 0.01$; N/S: not significant.

antibody appears to arrest Aβ$_{1-42}$ peptides in monomeric form, thus leading the accumulation of the signal. Finally, we analyzed synaptic connectivity in co-cultures treated with 8810 and 3D6 antibodies for 5 d prior to fixation (Fig. 3C). Similar to Fig. 2E, untreated CHO-APP^{LDN} co-cultures exhibited a strong (47.7%) decrease in the fraction of Syp puncta assigned by Homer puncta, without affecting the number of assignments. Treatment with 8810 antibody did not induce a significant difference relative to untreated controls in both cell types. However, treatment with 3D6 antibody completely blocked the effect of CHO-APP^{LDN} on synaptic connectivity. In summary, treatment with an antibody that prevents Aβ monomers from forming oligomers interfered with CHO-APP^{LDN}-secreted Aβ species and protected synapses from toxicity likely induced by low-MW oligomers. These findings highlight the potential use of our disease-on-a-chip model and synaptic connectivity analysis for assessing the synapto-protective effects of therapeutic compounds for AD, such as Aβ-targeting antibodies.

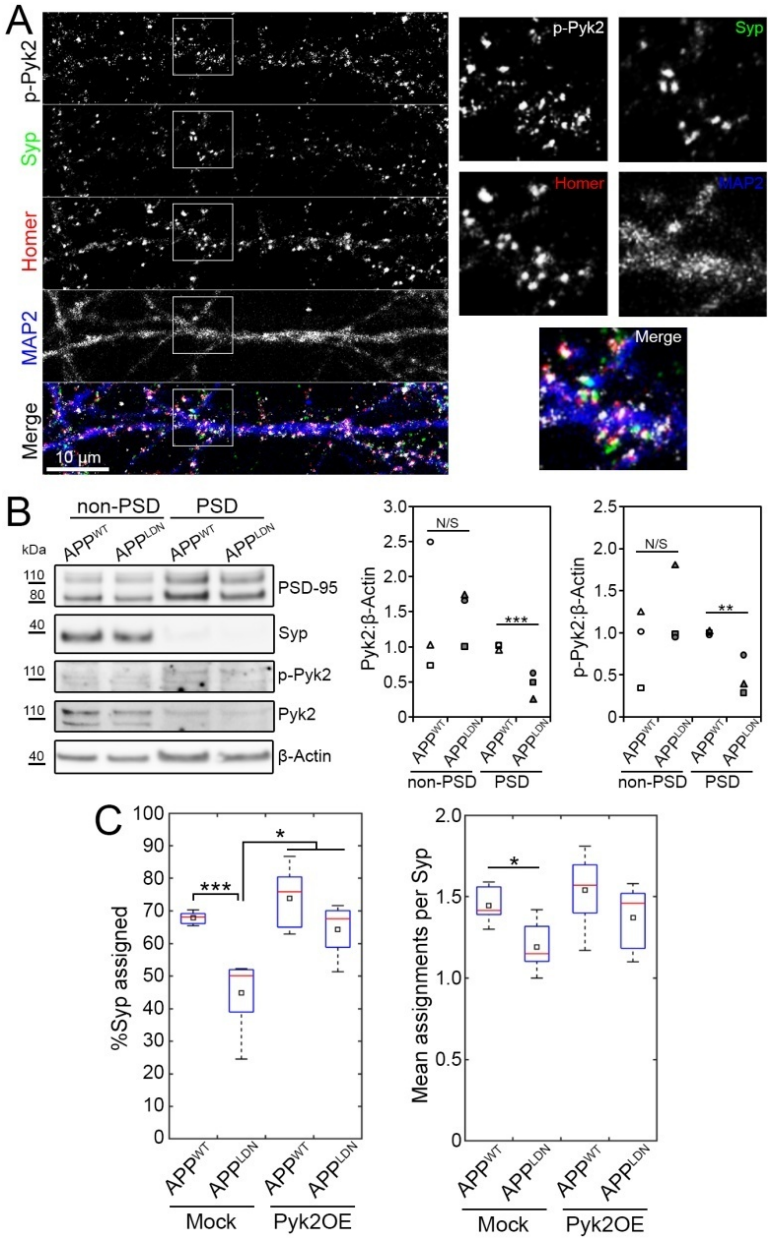

Figure 4. Pyk2 overexpression in postsynaptic neurons blocks the synaptotoxicity due to CHO-APP^{LDN} co-culture. **A.** An exemplary immunofluorescence image of the synaptic chamber at DIV14 showing phospho-Pyk2 Tyr402 (p-Pyk2), Synaptophysin 1 (Syp) Homer 1, and MAP2. Boxed areas are 2.4× magnified. **B.** Exemplary immunoblots and quantification of the postsynaptic (PSD) fraction following synaptosome extraction at DIV14 following 16 h-long treatment with the indicated CHO cell medium. N = 3 independent experiments. Student's *t*-test **C.** Synaptic read-outs following Pyk2 overexpression in postsynaptic neurons from DIV7 to DIV14. In box plots, red bars and black squares indicate sample median and mean, respectively. N = 5-7 devices from 3 independent experiments. Kruskal-Wallis ANOVA, followed by Wilcoxon rank-sum test. Error bars = SEM. * $p < 0.05$; ** $p < 0.01$; *** $p < 0.005$; N/S: not significant.

Pyk2 overexpression in "postsynaptic" neurons blocks CHO-APP^{LDN}-induced decrease in synapse connectivity

When phospho-Pyk2 (Tyr402) was immunostained alongside synaptic markers, we observed that signals localized to both pre- and postsynaptic puncta, with an increased tendency towards the latter (Fig. 4A). We extended our distance-based synaptic connectivity analysis to quantitatively analyze the distribution of

phospho-Pyk2 signals relative to identified synapses. Our data showed that 1.5-fold more phospho-Pyk2 puncta were localized near postsynaptic puncta than near presynaptic puncta (Fig. S6). To further confirm this observation, we conducted off-chip synaptosome extraction using primary cortical neurons treated with CHO cell media (Fig. 4B). We observed total Pyk2 and phospho-Pyk2 in both non-postsynaptic and postsynaptic fractions. There was no difference between neurons treated with CHO-APP^{LDN} medium and neurons treated with CHO-APP^{WT} medium in terms of Synaptophysin and PSD95 signals. (Fig. S7). However, CHO-APP^{LDN} medium caused significant decreases in the relative amounts of total Pyk2 and phospho-Pyk2 in the postsynaptic fraction (Fig. 4B).

Since the active form of Pyk2 was strongly associated with postsynapses and CHO-APP^{LDN} medium affected Pyk2 levels specifically in the postsynaptic fraction, we decided to take advantage of microfluidic compartmentalization and modulate Pyk2 expression in postsynaptic neurons. Since we observed a decrease in Pyk2 levels in the postsynaptic fraction upon treatment with CHO-APP^{LDN} media and a decrease in synaptic connectivity upon co-culture with CHO-APP^{LDN} cells, we hypothesized that Pyk2 was protective and its overexpression could rescue the detrimental effect of CHO-APP^{LDN} co-culture on synapses. We first verified the overexpression of Pyk2 off-chip via lentiviral transduction of the relevant cDNA (Fig. S8). Next, by using lentiviruses expressing fluorescent proteins, we confirmed that they were restricted to the target chambers (pre- or postsynaptic chambers; Fig. S9). Over-expression of Pyk2 in the postsynaptic chamber blocked the detrimental effect of CHO-APP^{LDN} co-culture on synaptic connectivity, as evidenced by 12.9% decrease in the fraction of Syp puncta assigned by Homer puncta (as compared to 33.9% decrease when overexpressing the control vector; Fig. 4C). Notably, synaptic connectivity in CHO-APP^{WT} co-cultures did not exhibit a significant change due to Pyk2 overexpression (8.7% increase in the fraction of Syp assigned), suggesting that the synaptoprotective effect of postsynaptic Pyk2 overexpression was linked to Aβ toxicity.

The role of Pyk2 in synapses appears to be complex, considering the seemingly opposite results of recent studies: Pyk2 has been shown to be required for long-term potentiation (LTP).[28] However, others have shown that Pyk2 is not required for LTP, but for long-term depression,[23, 38] and Pyk2 overexpression inhibits LTP.[38] The role of Pyk2 in Aβ toxicity has also been debated, where it has been shown to be deleterious [23] or protective [29] in mouse models. Our findings are in agreement with the notion that Pyk2 localizes to the postsynaptic compartment.[20] At the AD pathophysiological level, several of our observations fit well with the results of a recent *in vivo* study using AD-like mouse models: (i) decreased Pyk2 activity has been reported in 5XFAD mice,[29] although Pyk2 has also been shown to be activated in acute Aβ oligomer treatment on brain slices;[39, 40] (ii) rescue of Pyk2 expression improved the behavioral and synaptic molecular phenotypes of the double transgenic 5XFAD×Pyk$^{-/-}$ mouse model.[29] Interestingly, this rescue seems to have no impact on Aβ loads, suggesting that Pyk2 overexpression impacts pathophysiological processes downstream of Aβ production and amyloid deposition. This observation is in agreement with our results suggesting that Pyk2 overexpression may restrict Aβ-induced synaptotoxicity. Nevertheless, it is important to mention that the sparse literature on Pyk2's role in synapses is highly dependent on the model and calls for further *in vitro* and *in vivo* work.

Experimental

Oligimerization of synthetic Aβ peptides

Aβ peptides were oligomerized according to established protocols [4, 41] with minor modifications. The inactive control peptide (Aβ$_{42-1}$; Abcam; Cambridge, UK) has the same composition as the Aβ$_{1-42}$ peptide (California Peptide Research; Napa, CA) but with an inverted amino-acid sequence, and has been widely used as control for oligomeric Aβ$_{1-42}$ since it is also prone to oligomerization.[42-44] Aβ$_{1-42}$ and ICP were treated with hexafluoroisopropanol (HFIP; Sigma-Aldrich, Saint Louis, MO) to maintain the oligomeric structure and to

reduce fibril formation (Stine *et al.*, 2003), according to manufacturer's instructions. The peptides were resuspended in 1 ml HFIP and incubated for 1 h at RT, with occasional moderate vortexing, followed by sonication in water bath (Branson; Emerson Electric; St. Louis, MO) for 10 min. The solution was aliquoted into microcentrifuge tubes, let to evaporate in a chemical fume hood, dried with SpeedVac system (Thermo Fisher Scientific, Waltham, MA) for 30 min, and stored as desiccated peptide at -80°C. To produce oligomers, lyophilized, HFIP-treated aliquots of both peptides were resuspended in DMSO to reach 5 mM, mixed by pipetting, sonicated in water bath for 10 min, diluted to 100 µM in ice-cold D-PBS, followed by 30 s vortexing and 1 h incubation at 25°C. The solutions were aliquoted into microcentrifuge tubes and stored at -20°C for up to 4 weeks. Before adding to neurons, oligomeric peptide stocks were thawed, serial diluted to 100 nM in 2 % DMSO in PBS. Aβ42 concentrations up to 1 µM are considered non-lethal.[45, 46]

Microfluidic device design and fabrication

The microfluidic co-culture device was designed based on a previous tricompartmental neuron culture device.[32] The device consists of a 300 µm wide, 7.4 mm long central channel flanked by two 750 µm wide, 3.6 mm long side channels. All three channels are *ca.* 100 µm high. The left side channel (termed presynaptic) and the central channel (termed synaptic) are interconnected *via* 4 µm high, 450 µm long parallel microchannels that narrow from an entry width of 10 µm to an exit width of 3 µm. The right side channel (termed postsynaptic) and the synaptic chamber are also interconnected *via* parallel microchannels with identical dimensions, except that they were 75 µm long. One end of the synaptic chamber bifurcates into two branches, one of which terminates in a triangular shape. This terminus is connected to a diamond-shaped co-culture chamber (based on a previous design)[47] *via* 4 µm high, 10 µm wide, and 100 µm long parallel microchannels.

Master patterns were fabricated at the IEMN (Lille, France) *via* two-step photolithography.[48] Polydimethysiloxane (PDMS) pads, roughly 4 mm high, were replica molded. Access wells were punched at the termini of the central channel and the co-culture chamber, and of the side channels using 3 mm and 4 mm biopsy punches (Harris Unicore), respectively. The devices were permanently bonded to 24 mm × 50 mm glass coverslips (Menzel) *via* O_2 plasma (Diener, Ebhausen, Germany). Prior to cell culture, the devices were sterilized under UV light (Light Progress, Anghiari, Italy) for 30min, treated with 0.1 mg/mL PLL overnight, and rinsed with PBS.

Primary neuron culture

Culture media and supplements were from Thermo Fisher, unless mentioned otherwise. Primary neurons were obtained from P0 rats, according to previously described procedures.[49] Briefly, cortices and hippocampi were isolated from new-born rats, washed with ice-cold dissection medium (HBSS supplemented with HEPES, sodium pyruvate, and penicillin/streptomycin), and trypsinized (2.5%; at 37°C for 10 min). Trypsin was inactivated with dissociation medium (MEM supplemented with FBS, Glutamax, D-glucose (Sigma), MEM vitamins, and Pen/Strep), followed by DNase (5 mg/ml; Sigma) incubation for 1 min and wash with dissection medium. Media was replaced by dissociation medium and tissue was triturated with a fire-polished cotton-plugged Pasteur pipette to obtain a homogenous cell suspension, followed by centrifugation (200× *g* for 5 min). Cells were resuspended in culture medium (Neurobasal A supplemented with Glutamax and B_{27} neural supplement with antioxidants), counted, and plated at a density of 100,000 cells/cm^2 in 6- and 24-well plates for immunoblots and in 10 cm Petri dishes for synaptosome extraction. Plates were pre-coated with 0.1 mg/mL poly-l-lysine (Sigma) in 0.1M borate buffer (0.31% boric acid, 0.475% sodium tetraborate, pH = 8.5; Sigma) overnight at 37°C and rinsed thoroughly with water. Alternatively, cells were plated in pre-coated 384-well plates at 50,000 cells/cm² (*ca.* 4,000 cells/well) and in microfluidic devices at a density of *ca.* 8×10^5 cells/cm^2. After 20-24 h, culture media was replaced with supplemented Neurobasal A medium. 0.1% EDTA

(in H_2O) was added to the Petri dishes containing microfluidic devices to minimize evaporation. Cultures were maintained in a tissue culture incubator (Panasonic; Osaka, Japan) at 37°C and 5% CO_2.

Immunoblotting

Neurons were harvested in minimum volume of 200 µl/well in 6-well plates in ice-cold lysis buffer as described earlier.[50] Lysates were mixed with 4× LDS sample buffer (Novex; Thermo Fisher) and 10× reducing agent (Novex), sonicated, and boiled at 95°C for 10 min. Samples were loaded at maximum volume into 1.5 mm, 10-well, 4-12% Bis-Tris pre-cast NuPage gels (Novex), along with 5 µl MW marker (Novex Sharp pre-stained protein standard, Thermo Fisher). The gel was run with MES running buffer at 200 V for 45 min and transferred to 0.22 µm nitrocellulose membranes using the Trans-Blot Turbo transfer system (BioRad, Hercules, CA) using mixed MW method at 1.3 A and 25 V for 7 min. Membranes were blocked in TNT (0.05% Tween 20, 20 mM Tris-Base, 150 mM NaCl, pH = 8.0) containing 5% non-fat dry milk for 1 h at RT and washed 3× in TNT. Membranes were incubated with the following primary antibodies in SuperBlock T20 blocking buffer (Thermo Scientific) at 4°C overnight and washed 3× in TNT: rabbit anti-phospho-PTK2B (Cell Signaling Technology 3291; 1/1,000; Danvers, MA), rabbit anti-PTK2B (Sigma P3902; 1/1,000), and mouse anti-β-actin (Sigma A1978; 1/5,000). Membranes were then incubated with horseradish peroxidase-conjugated secondary antibodies (HRP-anti-Mouse and HRP-anti-rabbit; 1:5,000; Jackson ImmunoResearch, West Grove, PA) in TNT containing 5% non-fat dry milk for 1 h at RT and washed 3× in TNT. The membrane was revealed through chemiluminescence (Luminata Classico, EMD Merck Millipore) and imaged with Amersham Imager 600 (GE Healthcare, Mississauga, Canada). The images were quantified with ImageQuantTL Software (GE Healthcare).

Culture of CHO cells and analysis of their media

CHO cell lines (CHO-pcDNA4, -APP^{WT} and -APP^{LDN}) were maintained according to previously described procedures.[34] Cells were grown in CHO growth medium: DMEM/Ham's F-12 1:1 medium, supplemented with 10% heat-inactivated fetal bovine serum (FBS), 0.2% Pen/Strep, 2% HT supplement, and 300 µM Proline (Sigma). To stimulate Aβ production, the growth medium was replaced with CHO-NBA medium: phenol red-free Neurobasal A (Gibco) supplemented with 0.2% Pen/Strep, 2% HT supplement, and 300 µM Proline.
For media collection, cells were grown in 10 cm Petri dishes or in 6-well plates until they reached 80% confluence, at which point the maintenance medium was rinsed with PBS and replaced with the stimulation medium. After 48 h of stimulation, the medium was collected into 15 mL Falcon tubes and centrifuged at 4,000× *g* and 4°C for 10 min to remove the debris. The supernatant was loaded into a 3 kDa spin column (Amicon Ultra; Merck), equilibrated with Neurobasal (without serum or Phenol Red) at 4,000× *g* and 4°C for 10 min, and concentrated at 4,000× *g* and 4°C for 1 h. Western blotting of conditioned media was performed as described with the following exceptions: the transferred membrane was boiled for 5 min in PBS and Luminata Crescendo (Millipore) was used as the HRP substrate. Anti-$A\beta_{1-42}$ (clone 6E10; 1:1000; Sigma) was used as primary antibody.

Exposure of neurons to conditioned media

Total protein concentration in the conditioned media collected from different CHO cell lines (CHO-pcDNA4, -APP^{WT} and -APP^{LDN}) was assessed using the Pierce BCA Protein Assay Kit (Thermo Fisher) and adjusted to 100 µg/µL with supplemented CHO-NBA medium. 10 µL of conditioned media (per well) was added to primary neuronal cultures grown in 384-well plates (containing 40 µL of culture medium per well) at DIV14,

DIV18, DIV19, DIV20, and DIV21 (6 h prior to media collection). Media from these wells (8 wells per condition) were collected into a new 384-well plate prior to quantification of Aβ peptides.

Co-culture of neurons with CHO cells

CHO cells were seeded in the co-culture chamber at a density of *ca.* 1.3×10^5 cells/cm^2 and maintained in a tissue culture incubator (5% CO_2; 37°C) in CHO medium. On the day of primary neuron culture, the medium was replaced with CHO-NBA medium supplemented with 1% Glutamax and 2% B_{27} neural supplement with antioxidants. Primary neurons were seeded in the pre- and postsynaptic chambers. At DIV1, the medium in all wells was replaced with fresh supplemented CHO-NBA medium. Every 3-4 days, the medium in the access wells of the co-culture chamber was replaced with fresh medium, whereas the medium in other wells were only topped up with fresh medium.

Lentiviral transductions

At DIV7, neurons cultured in the postsynaptic chamber were transducted with lentiviruses according to established methods.[49] To avoid transduction of CHO cells and the neurons in the presynaptic chamber, a hydrostatic pressure gradient was formed across the microchannels separating synaptic and postsynaptic chambers. The following lentiviruses were used for transduction: Mission shRNA vectors (Sigma) pLenti6/Ubc/v5-DEST (Invitrogen, Carlsbad, CA) empty (Mock) or including human PTK2B cDNA sequences, synthesized via the GeneArt service (Thermo Fisher). LifeAct-Ruby (pLenti.PGK.LifeAct-Ruby.W; RRID: Addgene_51009) and LifeAct-GFP (pLenti.PGK.LifeAct-GFP.W; RRID: Addgene_51010) were kind gifts from Rusty Lansford. Viral transduction was performed at multiplicity of infection (MOI) of 4. Constructs were diluted in pre-warmed, supplemented CHO-NBA medium containing 2 µg/mL (5×) Polybrene (hexadimethrine bromide; Sigma). Media from pre- and postsynaptic wells were collected in a common tube. 25 µL, 15 µL, and 20 µL of the collected media were returned to each presynaptic, synaptic, and postsynaptic well, respectively. 10 µL of virus suspension was added to one of the postsynaptic wells. Neurons were incubated with viral particles for 6 h before the wells were topped up with the remainder of the collected media. Co-cultures were maintained as described earlier.

Alpha-LISA measurements

Alpha-LISA is a highly sensitive, quantitative assay based on biotinylated antibody bound to streptavidin-coated donor beads and antibody-conjugated acceptor beads. In the presence of the analyte, the beads come into close proximity such that the excitation of the donor beads triggers a cascade of energy transfer in the acceptor beads, resulting in a sharp peak of light emission at 615 nm. We used Alpha-LISA kits specific to human $A\beta_{1\text{-}X}$ and $A\beta_{1\text{-}42}$ (AL288C and AL276C, respectively; PerkinElmer, Waltham, MA) to measure the amount of $A\beta_{1\text{-}X}$ and $A\beta_{1\text{-}42}$ in culture media. The human Aβ analyte standard was diluted in CHO-NBA medium. For the assay, we first added 5 µL of cell culture supernatant or standard solution into an Optiplate-96 microplate (PerkinElmer). We then added 5 µL of 10× mixture including acceptor beads and biotinylated antibody. Following incubation at RT for 60 min, we added 40 µL of 1.25× donor beads and incubated at RT for 60 min. We measured the fluorescence using an EnVision-Alpha Reader (PerkinElmer) at 680 nm excitation and 615 nm emission wavelengths. In experiments where conditioned media was added to primary neurons in 384-well plates, 2 µL of collected media was transferred to an Optiplate-384 (PerkinElmer) and Alpha-LISA was performed using reduced volumes: 2 µL of sample or standard, 2 µL of acceptor beads and biotinylated antibody mix, and 16 µL of donor beads.

ELISA measurements

The sandwich ELISA was performed according to the manufacturer's protocol. We used microtiter plates pre-coated with anti-human $A\beta_{35-40}$ antibody (clone 1A10; RE59781, IBL) and anti-human $A\beta_{38-42}$ (clone 1C3; RE59721, IBL) to detect $A\beta_{1-40}$ and $A\beta_{X-42}$, respectively. Plates were incubated overnight at 4°C with 100 µL cell culture supernatant or with standards. The bound antigen was detected by incubating the wells with 100 µL of 30× mixture containing the HRP-conjugated anti-human Aβ antibodies (clone 82E1 for $A\beta_{1-40}$ and clone 12B2 for $A\beta_{X-42}$) for 60 min at 4°C. Signal was revealed by incubating with the TMB substrate for 30 min at RT in the dark and stopping the enzymatic reaction with the TMB stop solution containing 1N H_2SO_4. Signal intensity was read immediately at 405 nm via a microplate reader (PowerWave XS2, BioTek Instruments, Winooski, VT).

Immunocytochemistry and microscopy

Co-cultures were fixed at DIV14 in PBS containing 4% paraformaldehyde for 20 min at RT and permeabilized with 0.3% (v/v) Triton X-100 in PBS for 5 min. After blocking in 5% (w/v) normal donkey serum, samples were incubated overnight at 4°C with the following antibodies: anti-MAP2 (188011; Synaptic Systems, Göttingen, Germany); anti-Homer (160006; Synaptic Systems) and anti-PYK2 phospho-Y402 (ab4800; Abcam, Cambridge, UK). Cells were rinsed with PBS and incubated with the following secondary antibodies for 2 h at RT: Dylight 405 Donkey anti-mouse (715-475-151; Jackson); AlexaFluor 647 donkey anti-rabbit (711-605-152; Jackson) and AlexaFluor 594 Donkey anti-chicken (703-585-155; Jackson). Cells were rinsed with PBS and incubated with mouse monoclonal anti-Synaptophysin 1 pre-labeled with Oyster 488 (101011C2; Synaptic Systems) for 2 h at RT. Cells were rinsed with PBS and microfluidic devices were topped with 90% glycerol.

Samples were imaged with a LSM 880 confocal microscope (Zeiss, Oberkochen, Germany) equipped with a 63× 1.4 NA objective. Images were acquired at zoom 2 in *z*-stacks of 0.5 µm interval. Typically, 4 images were acquired per device from the synapse chamber near the postsynaptic chamber such the image contains multiple dendrites. Images were deconvoluted using AutoQuantX3 software (BitPlane, Zurich, Switzerland) for synaptic connectivity analysis.

In a subset of experiments, neurons were plated only in the presynaptic chamber, only in the postsynaptic chamber, or only in the synaptic chamber. Neurons were fixed and immunostained at DIV14 as described to reveal nuclei, GFAP (ABD95; Millipore) and β3-tubulin (MAB1637, Millipore). All chambers were imaged using a Zeiss AxioObserver Z1 epifluorescense microscope equipped with a Prime 95B Scientific CMOS (Photometrics, Tucson, AZ) camera and 32× objective. The integrated density (pixel values × area) of the β3-tubulin signal was quantified in all chambers, at a distance between 50 and 200 µm from the entries and exits of the microchannels. Neurite penetration rates for short and long microchannels (in the forward and reverse directions) were estimated by taking the ratio of the β3-tubulin integrated density signals obtained from the emitting and receiving chambers. The ratio between the penetration rates between forward and reverse directions was defined as the directionality ratio.

Quantification of synapse integrity

We developed an image analysis workflow based on image segmentation using Imaris software (BitPlane) and assignment of postsynaptic signals to the nearest presynaptic signal using a custom Matlab (Mathworks; Natick, MA) code. Briefly, signals obtained for pre- and postsynaptic structures were first segmented into distinct volumes using the surfaces function of Imaris in the batch mode that permits the same parameters to be applied to all images (Fig. S2A-S2D). Postsynaptic spots were then assigned to the nearest presynaptic spot (according to the distance between centers of mass) within a predefined cut-off distance (Fig. S2E). We empirically determined the cut-off distance by testing a range on a large set of control cultures (Fig. S2F-

S2G). The average number and distance of such assignments and the fraction of pre- and postsynaptic signals without any assignments were used as output parameters. Note that a small fraction of control samples for CHO-APP^{WT} and CHO-APP^{LDN} co-cultures (2 devices each) overlap in results reported in Fig. 2E and Fig. 3C.

Analysis of phospo-Pyk2 signals relative to synapses

We extended the image analysis workflow to analyze the positions of phospho-Pyk2 puncta relative to the positions of identified synapses. Postsynaptic spots were first assigned to the nearest presynaptic spot as described. For each postsynaptic-to-presynaptic assignment, or "synapse", we defined the midpoint as being equidistant to pre- and postsynaptic puncta. We next defined pre- and postsynaptic zones, by spanning two right circular cones with 45° polar angle where the midpoint is the apex. We then associated phospho-Pyk2 puncta with the nearest "synapse" as long as it was within a pre-defined cut-off distance from the midpoint and categorized these associations as presynaptic, postsynaptic, or other (neither pre- nor postsynaptic). We then calculated the average number of phospho-Pyk2 puncta associated with each "synapse".

Synaptosome extraction

To verify the presence of proteins at the synaptic level we did a subcellular fractionation as previously described.[51] Briefly, cortical neurons were cultured in 10 cm Petri dishes as described ($3.5\text{-}4.0 \times 10^7$ neurons per condition). At DIV13, neurons were exposed to CHO-APP^{WT} or CHO-APP^{LDN} media for 18 h (final $A\beta_{1\text{-}X}$ concentration: 40 nM). At the end of this treatment, neurons were lysed, reconstituted in a solution (0.32 M sucrose and 10 mM HEPES, pH = 7.4), and centrifuged at 1,000× *g* for 10 min to remove nuclei and debris. The supernatant was centrifuged at 12,000× *g* for 20 min to remove the cytosolic fraction. The pellet was reconstituted in a second solution (4 mM HEPES, 1 mM EDTA, pH = 7.4) and was centrifuged 2× at 12,000× *g* for 20 min. The new pellet was reconstituted in a third solution (20 mM HEPES, 100 mM NaCl, 0.5% Triton X-100, pH = 7.2) for 1 h at 4°C and centrifuged at 12,000× *g* for 20 min. The supernatant collected corresponds to the non-PSD fraction (Triton-soluble). The remaining pellet was reconstituted in a fourth solution (20 mM HEPES, 0.15 mM NaCl, 1% Triton X-100, 1% deoxycholicacid, 1% SDS, pH = 7.5) for 1 h at 4°C and was centrifuged at 10,000× *g* for 15 min to obtain a supernatant containing the PSD fraction (Triton-insoluble). The fractions obtained were then analyzed by WB.

Conclusions

In conclusion, our microfluidic co-culture device provides an *in vitro* model of Aβ synaptotoxicity based on exposing synapses of primary hippocampal neurons to cell-secreted $A\beta_{1\text{-}42}$ peptides. This disease-on-a-chip model is highly relevant to AD in several aspects: (i) long-term, low-dose exposure to organic Aβ forms is preferable over acute treatments with synthetic oligomers at high concentrations; (ii) isolating synapses in a separate microfluidic chamber facilitates the analysis of synaptic connectivity *via* immunostaining pre- and postsynaptic markers without the interference of cell bodies; (iii) providing exclusive access to pre- and postsynaptic neurons to selectively under- or overexpress AD genetic risk factors therein helps dissect their potential roles in pre- and postsynaptic compartments. Deciphering the mechanisms by which the genetic risk factors contribute to AD pathology will help develop targeted therapies based on genetic information.

Acknowledgements

The authors thank the BICeL platform of the Institut Biologie de Lille. The authors thank Laurent Pradier and Philippe Bertrand at Sanofi for fruitful discussions. The authors thank Karine Blary at the IEMN Lille for the microfabrication work. This work was partly supported by the French RENATECH network. This study was funded by INSERM, Institut Pasteur de Lille, the EU Joint Programme – Neurodegenerative Diseases Research (JPND; 3DMiniBrain), Agence Nationale de la Recherche (ANR-19-CE16-0020), and Fondation Vaincre Alzheimer (FR-17006p). This work was also funded by the Lille Métropole Communauté Urbaine and the French government's LABEX DISTALZ program (Development of innovative strategies for a transdisciplinary approach to Alzheimer's disease). The authors thank the vectorology platform Transbiomed for lentivirus production.

References

1. R. M. Nisbet, J. C. Polanco, L. M. Ittner and J. Gotz, *Acta Neuropathol*, 2015, **129**, 207-220.
2. B. De Strooper, *Physiol Rev*, 2010, **90**, 465-494.
3. J. Hardy and D. J. Selkoe, *Science*, 2002, **297**, 353-356.
4. W. B. Stine, Jr., K. N. Dahlgren, G. A. Krafft and M. J. LaDu, *J Biol Chem*, 2003, **278**, 11612-11622.
5. K. N. Dahlgren, A. M. Manelli, W. B. Stine, Jr., L. K. Baker, G. A. Krafft and M. J. LaDu, *J Biol Chem*, 2002, **277**, 32046-32053.
6. R. Resende, E. Ferreiro, C. Pereira and C. Resende de Oliveira, *Neuroscience*, 2008, **155**, 725-737.
7. A. Deshpande, E. Mina, C. Glabe and J. Busciglio, *J Neurosci*, 2006, **26**, 6011-6018.
8. I. L. Ferreira, L. M. Bajouco, S. I. Mota, Y. P. Auberson, C. R. Oliveira and A. C. Rego, *Cell Calcium*, 2012, **51**, 95-106.
9. T. L. Spires-Jones and B. T. Hyman, *Neuron*, 2014, **82**, 756-771.
10. I. Benilova, E. Karran and B. De Strooper, *Nat Neurosci*, 2012, **15**, 349-357.
11. A. H. Brody and S. M. Strittmatter, *Adv Pharmacol*, 2018, **82**, 293-323.
12. P. T. Lansbury, Jr., *Proc Natl Acad Sci U S A*, 1999, **96**, 3342-3344.
13. S. W. Scheff, D. A. Price, F. A. Schmitt, S. T. DeKosky and E. J. Mufson, *Neurology*, 2007, **68**, 1501-1508.
14. F. J. Sepulveda, J. Parodi, R. W. Peoples, C. Opazo and L. G. Aguayo, *PLoS One*, 2010, **5**, e11820.
15. S. Hong, V. F. Beja-Glasser, B. M. Nfonoyim, A. Frouin, S. Li, S. Ramakrishnan*, et al.*, *Science*, 2016, **352**, 712-716.
16. J. W. Um, H. B. Nygaard, J. K. Heiss, M. A. Kostylev, M. Stagi, A. Vortmeyer*, et al.*, *Nat Neurosci*, 2012, **15**, 1227-1235.
17. Q. Wang, D. M. Walsh, M. J. Rowan, D. J. Selkoe and R. Anwyl, *J Neurosci*, 2004, **24**, 3370-3378.
18. B. W. Kunkle, B. Grenier-Boley, R. Sims, J. C. Bis, V. Damotte, A. C. Naj*, et al.*, *Nat Genet*, 2019, **51**, 414-430.
19. J. C. Lambert, C. A. Ibrahim-Verbaas, D. Harold, A. C. Naj, R. Sims, C. Bellenguez*, et al.*, *Nat Genet*, 2013, **45**, 1452-1458.
20. A. Giralt, V. Brito, Q. Chevy, C. Simonnet, Y. Otsu, C. Cifuentes-Diaz*, et al.*, *Nat Commun*, 2017, **8**, 15592.
21. S. A. Ojelade, T. V. Lee, N. Giagtzoglou, L. Yu, B. Ugur, Y. Li*, et al.*, *Cell Rep*, 2019, **28**, 1799-1813.e1795.
22. B. Schurmann, D. P. Bermingham, K. J. Kopeikina, K. Myczek, S. Yoon, K. E. Horan*, et al.*, *Mol Psychiatry*, 2019.
23. S. V. Salazar, T. O. Cox, S. Lee, A. H. Brody, A. S. Chyung, L. T. Haas*, et al.*, *J Neurosci*, 2019, **39**, 758-772.
24. F. Eysert, A. Coulon, E. Boscher, A. C. Vreulx, A. Flaig, T. Mendes*, et al.*, *bioRxiv*, 2019, 767194.
25. P. Dourlen, D. Kilinc, N. Malmanche, J. Chapuis and J. C. Lambert, *Acta Neuropathol*, 2019, **138**, 221-236.
26. M. Kollmer, W. Close, L. Funk, J. Rasmussen, A. Bsoul, A. Schierhorn*, et al.*, *Nat Commun*, 2019, **10**, 4760.
27. J. A. Bartos, J. D. Ulrich, H. Li, M. A. Beazely, Y. Chen, J. F. Macdonald*, et al.*, *J Neurosci*, 2010, **30**, 449-463.
28. Y. Huang, W. Lu, D. W. Ali, K. A. Pelkey, G. M. Pitcher, Y. M. Lu*, et al.*, *Neuron*, 2001, **29**, 485-496.
29. A. Giralt, B. de Pins, C. Cifuentes-Diaz, L. Lopez-Molina, A. T. Farah, M. Tible*, et al.*, *Exp Neurol*, 2018, **307**, 62-73.
30. A. M. Taylor, D. C. Dieterich, H. T. Ito, S. A. Kim and E. M. Schuman, *Neuron*, 2010, **66**, 57-68.
31. A. Virlogeux, E. Moutaux, W. Christaller, A. Genoux, J. Bruyere, E. Fino*, et al.*, *Cell Rep*, 2018, **22**, 110-122.
32. D. Kilinc, A. Blasiak, J. J. O'Mahony and G. U. Lee, *Sci Rep*, 2014, **4**, 7128.
33. J. M. Peyrin, B. Deleglise, L. Saias, M. Vignes, P. Gougis, S. Magnifico*, et al.*, *Lab Chip*, 2011, **11**, 3663-3673.

34. M. V. Guillot-Sestier, C. Sunyach, S. T. Ferreira, M. P. Marzolo, C. Bauer, A. Thevenet*, et al.*, *J Biol Chem*, 2012, **287**, 5021-5032.
35. M. D. Santin, M. E. Vandenberghe, A. S. Herard, L. Pradier, C. Cohen, T. Debeir*, et al.*, *Front Aging Neurosci*, 2016, **8**, 55.
36. R. Vandenberghe, J. O. Rinne, M. Boada, S. Katayama, P. Scheltens, B. Vellas*, et al.*, *Alzheimers Res Ther*, 2016, **8**, 18.
37. L. A. Miles, G. A. Crespi, L. Doughty and M. W. Parker, *Sci Rep*, 2013, **3**, 1302.
38. H. Hsin, M. J. Kim, C. F. Wang and M. Sheng, *J Neurosci*, 2010, **30**, 11983-11993.
39. L. T. Haas, S. V. Salazar, M. A. Kostylev, J. W. Um, A. C. Kaufman and S. M. Strittmatter, *Brain*, 2016, **139**, 526-546.
40. L. T. Haas and S. M. Strittmatter, *J Biol Chem*, 2016, **291**, 17112-17121.
41. K. H. Chang, F. Vincent and K. Shah, *J Cell Sci*, 2012, **125**, 5124-5137.
42. G. Mairet-Coello, J. Courchet, S. Pieraut, V. Courchet, A. Maximov and F. Polleux, *Neuron*, 2013, **78**, 94-108.
43. D. T. Walsh, R. M. Montero, L. G. Bresciani, A. Y. Jen, P. D. Leclercq, D. Saunders*, et al.*, *Neurobiol Dis*, 2002, **10**, 20-27.
44. K. Xiong, H. Cai, X. G. Luo, R. G. Struble, R. W. Clough and X. X. Yan, *Exp Brain Res*, 2007, **181**, 435-446.
45. B. L. Kelly and A. Ferreira, *Neuroscience*, 2007, **147**, 60-70.
46. I. Kuperstein, K. Broersen, I. Benilova, J. Rozenski, W. Jonckheere, M. Debulpaep*, et al.*, *Embo J*, 2010, **29**, 3408-3420.
47. D. Kilinc, J. Schwab, S. Rampini, O. W. Ikpekha, A. Thampi, A. Blasiak*, et al.*, *Integr Biol (Camb)*, 2016, **8**, 39-49.
48. A. Blasiak, G. U. Lee and D. Kilinc, *ACS Chem Neurosci*, 2015, **6**, 1578-1590.
49. M. Sartori, T. Mendes, S. Desai, A. Lasorsa, A. Herledan, N. Malmanche*, et al.*, *Acta Neuropathol*, 2019, **138**, 631-652.
50. J. Chapuis, A. Flaig, B. Grenier-Boley, F. Eysert, V. Pottiez, G. Deloison*, et al.*, *Acta Neuropathol*, 2017, **133**, 955-966.
51. M. L. Frandemiche, S. De Seranno, T. Rush, E. Borel, A. Elie, I. Arnal*, et al.*, *J Neurosci*, 2014, **34**, 6084-6097.

Supplementary Figures

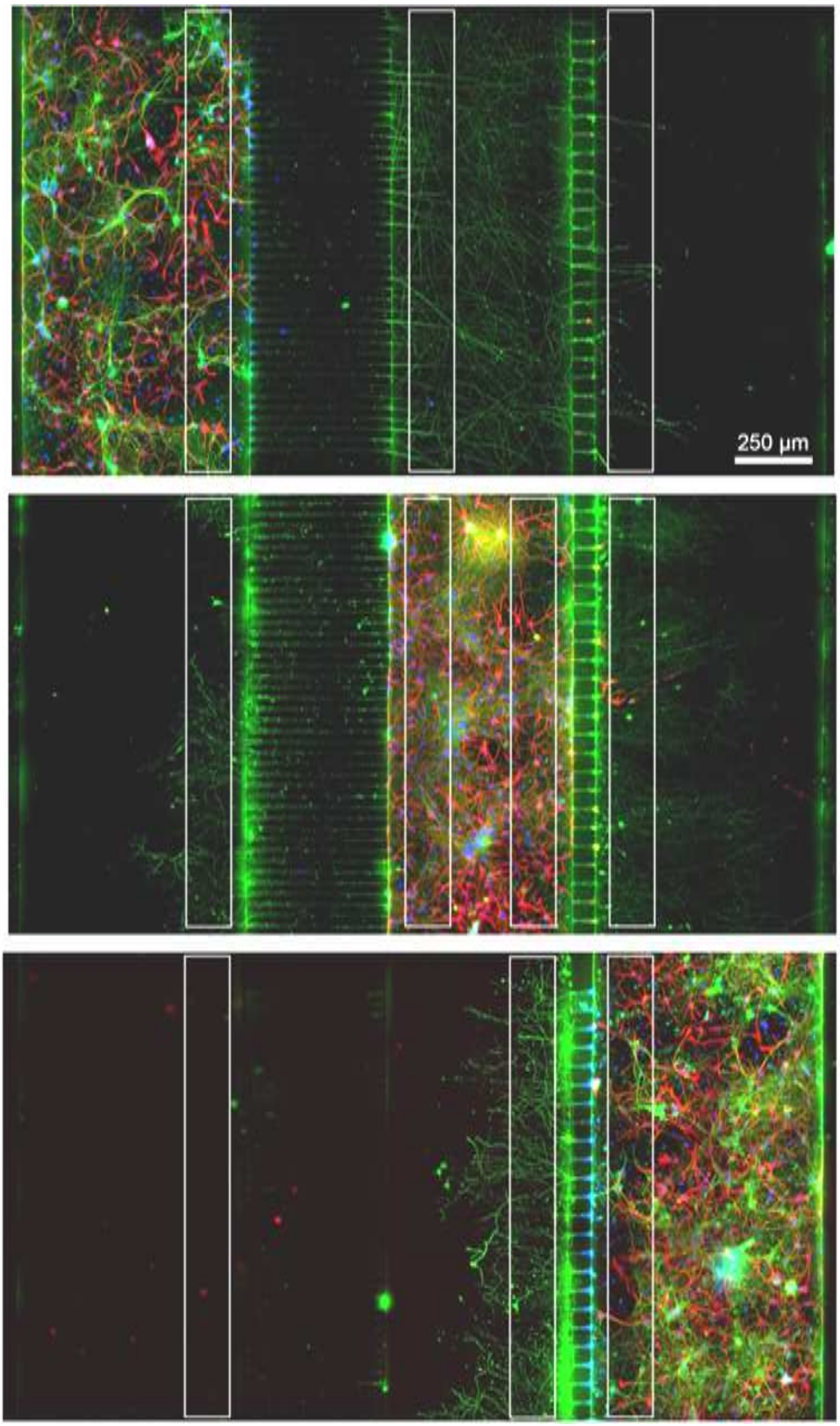

Figure S1. Exemplary images of microfluidic devices where primary neurons were plated in only one chamber. β3-tubulin (green), Hoechst (blue), and GFAP (red) staining at DIV14. White rectangles indicate regions where β3-tubulin staining intensity was measured to calculate penetration ratios.

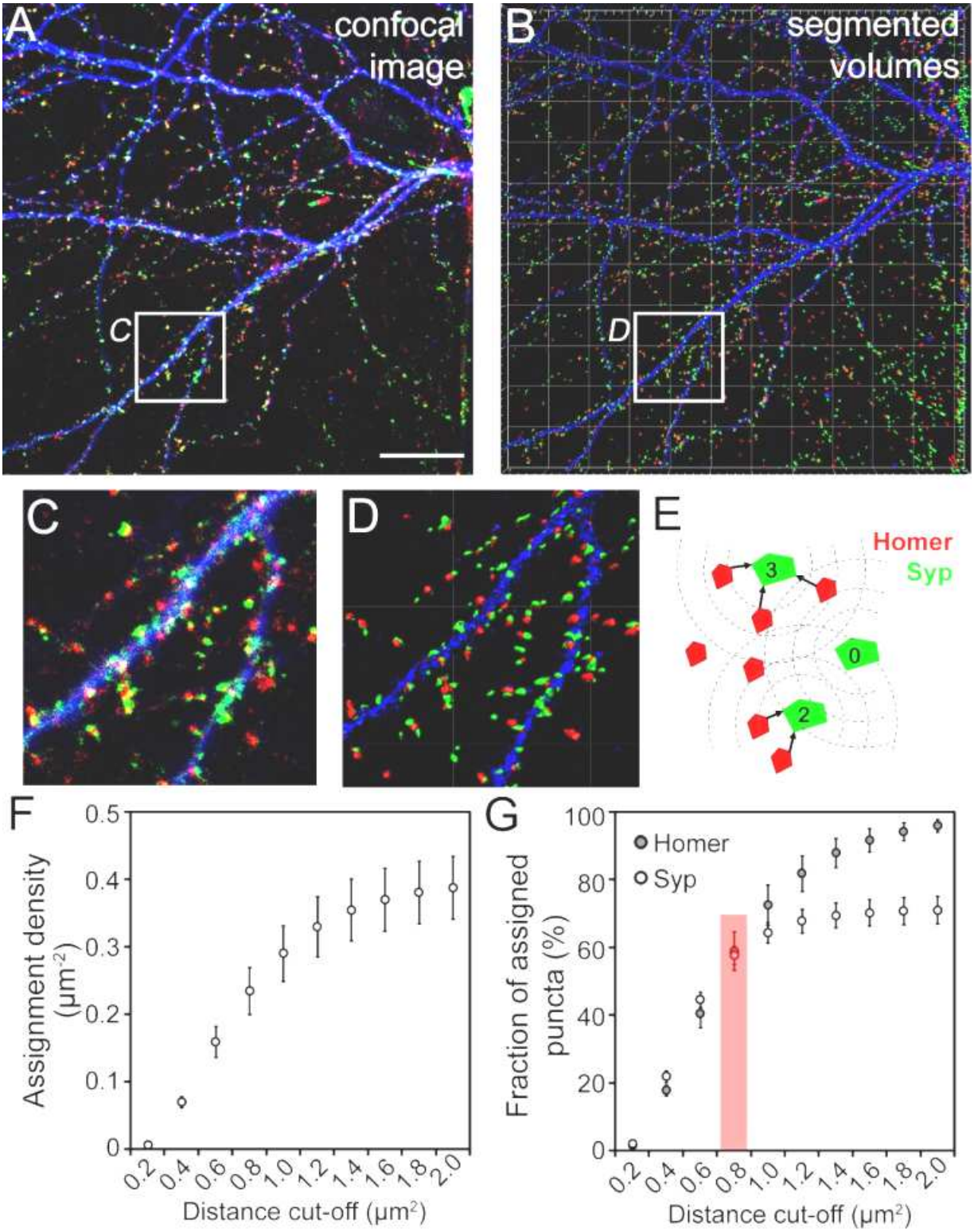

Figure S2. Synapse analysis workflow and the determination of the distance cut-off. **A.** An exemplary dendrite in the synaptic chamber. Image shows the maximum intensity projection of Homer 1 (red), Synaptophysin 1 (green), and MAP2 (blue) stains. **B.** Segmentation of the same image in Imaris. **C-D.** Marked areas in *A* and *B*, respectively, magnified 3.5×. **E.** Principle of assigning postsynaptic (Homer) to presynaptic (Syp) puncta based on proximity. Numbers indicate the number of assignments for each presynaptic puncta. **F.** Synaptic assignment density as a function of distance cut-off. **G.** Fractions of assigned pre- and postsynaptic puncta as a function of distance cut-off, showing that Syp assignments saturate at around 1.0 µm for the dataset analyzed. N = 9 microfluidic devices from 4 independent cultures; 5-8 images per device. Bars show SEM.

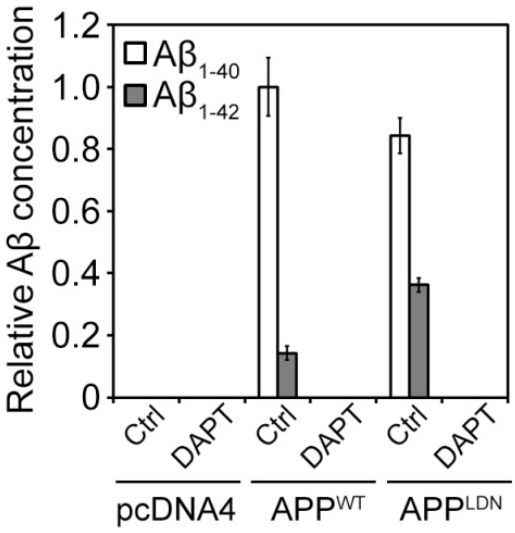

Figure S3. Relative $A\beta_{1-42}$ concentration in off-chip CHO cell media quantified via ELISA. γ-secretase inhibitor DAPT was applied at 18 μg/mL for 5 d. Data normalized to APP^{WT} control condition. As the sample was concentrated prior to $A\beta_{1-42}$ measurement, $A\beta_{1-42}$ levels cannot be directly compared to $A\beta_{1-40}$ levels.

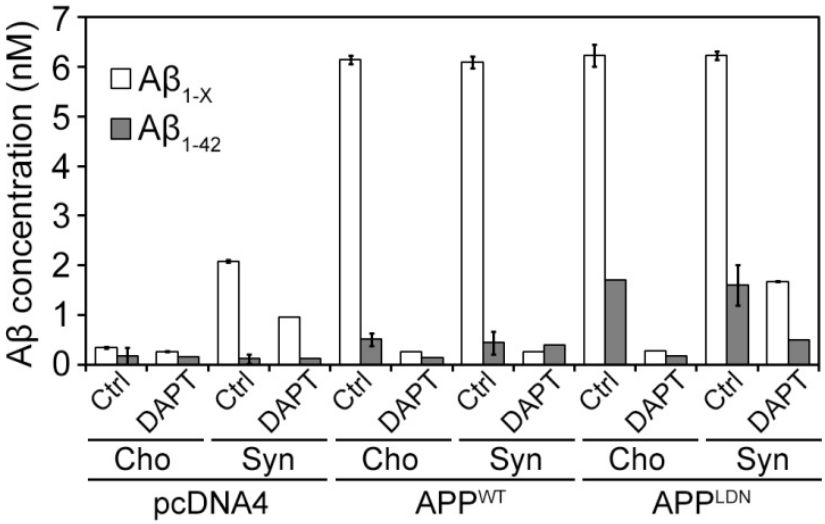

Figure S4. Concentration of $A\beta_{1-X}$ and $A\beta_{1-42}$ in the media collected from different reservoirs of the co-culture device at DIV14 measured via Alpha-LISA. Cho: Co-culture chamber; Syn: Synaptic chamber. Note that data for the synaptic chamber are identical to what is shown in Figure 2D.

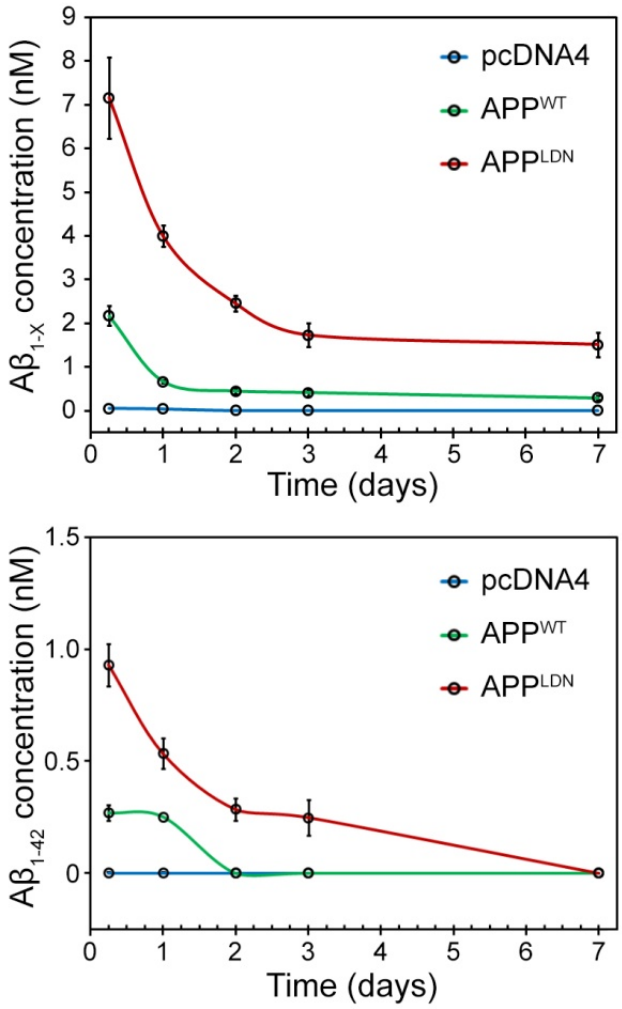

Figure S5. Concentration of $A\beta_{1\text{-}X}$ and $A\beta_{1\text{-}42}$ in the media collected from primary neurons cultured in 384-well plates and exposed to CHO cell-conditioned media for 6 h to 7 d. Concentration was determined via Alpha-LISA using 6-8 wells per condition.

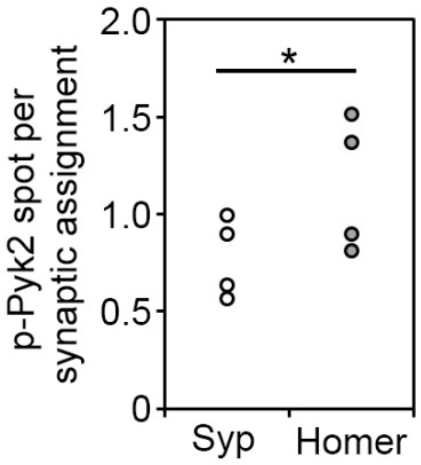

Figure S6. Localization of phospho-Pyk2 Tyr402 (p-Pyk2) puncta relative to synapses. Each Homer spot was assigned to the nearest Synaptophysin (Syp) spot within cut-off distance of 1.0 µm. Each p-Pyk2 spot was assigned to the nearest "synapse", i.e., midpoint between Syp and Homer spots, within cut-off distance of 1.5 µm. Such assignments were then categorized as presynaptic or postsynaptic, if they were within 45° cones emanating from the midpoint towards Syp and Homer spots, respectively. N = 4 independent experiments. * $p < 0.01$; paired t-test.

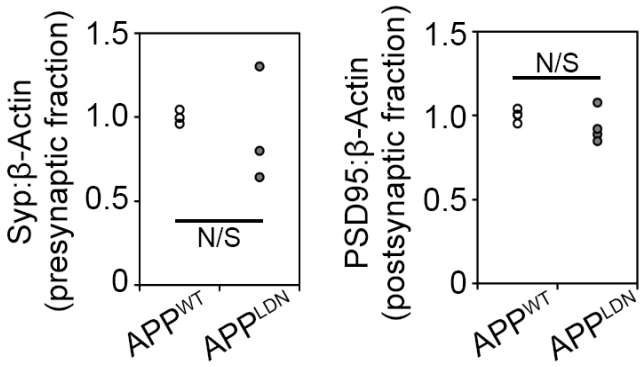

Figure S7. Quantification of synaptic markers in the synaptosomal fraction. Synaptophysin (Syp) in the presynaptic fraction and PSD95 in the postsynaptic fraction for primary neuronal cultures exposed to media collected from CHO-APP^{WT} and CHO-APP^{LDN} cultures. N/S: not significant.

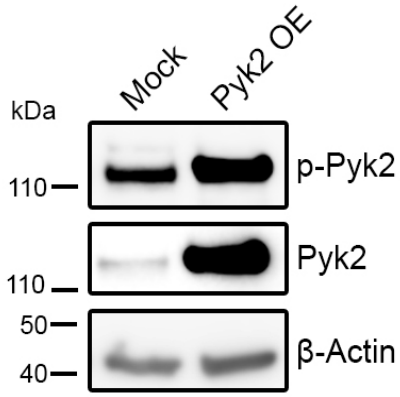

Figure S8. An exemplary immunoblot demonstrating the overexpression of Pyk2 in primary neuronal cultures at DIV14 following lentiviral transduction at DIV7.

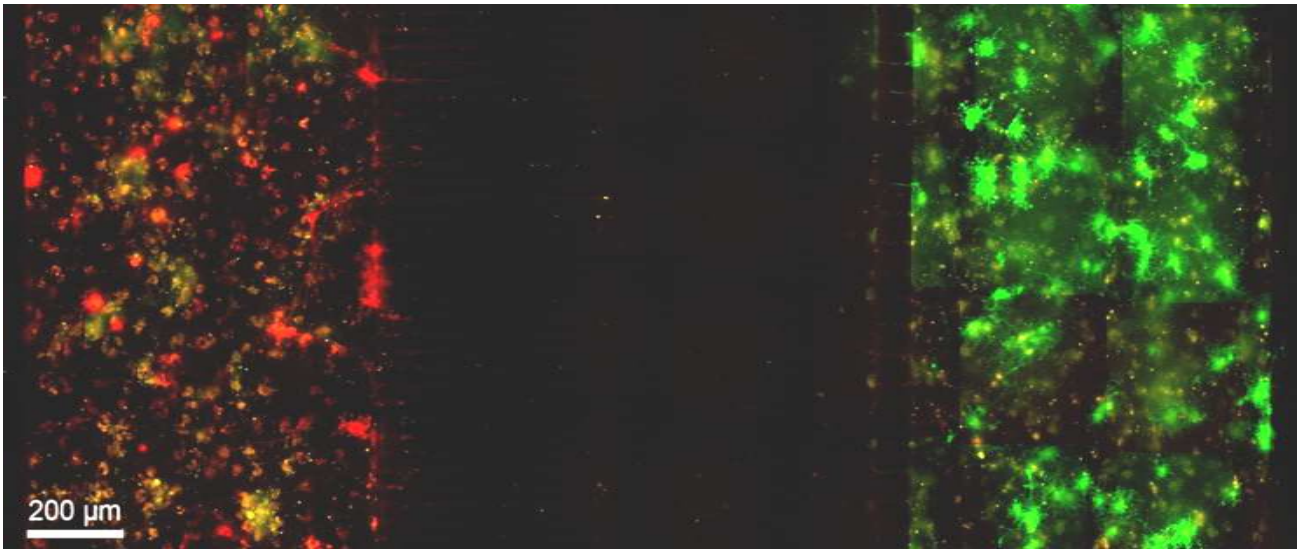

Figure S9. Demonstration of isolated lentiviral treatments at DIV14. Cells cultured in pre- and postsynaptic chambers were transducted at DIV7 with lentiviruses to express LifeAct-ruby (red) and LifeAct-GFP (green), respectively.